UNIVERSIDADE D
COIMBRA

Ângela Marina das Neves Calhau

Computational model for the adhesion between red blood cells and their deformation

Dissertation in the context of the Master in Biomedical Engineering, Specialization in Clinical Informatics and Bioinformatics, advised by Professor Rui Travasso (PhD.) and Filomena Carvalho (PhD.) and presented to the Physics Department of the Faculty of Sciences and Technology of the University Of Coimbra

February of 2024

1 2 9 0

FACULDADE DE CIÊNCIAS E TECNOLOGIA
UNIVERSIDADE D COIMBRA

Ângela Marina das Neves Calhau

Computational model for the adhesion between red blood cells and their deformation

Dissertation in the context of the Master in Biomedical Engineering, Specialization in Clinical Informatics and Bioinformatics, advised by Professor Rui Travasso (PhD.) and Filomena Carvalho (PhD.) and presented to the Physics Department of the Faculty of Sciences and Technology of the University Of Coimbra

Supervisors:
Prof. Dr. Rui Travasso (CFis/UC)
Prof. Dr. Filomena Carvalho (iMM/UL)

Coimbra, 2024

This work was developed under the project PTDC/EMD-TLM/7289/2020, in collaboration with:

Centre for Physics of the University of Coimbra

Faculty of Medicine of the University of Lisbon

Institute of Molecular Medicine

Agradecimentos

Começo por agradecer aos meus orientadores, ao Prof. Dr. Rui Travasso e à Prof. Dra. Filomena Carvalho, pela confiança que me depositaram e por todo o apoio, dedicação e orientação que me prestaram ao longo de todo o trabalho desta Tese de Mestrado. Gostaria também de agradecer aos colegas do grupo de investigação pelas reuniões e discussões que me permitiram melhorar e evoluir ao longo deste gratificante período académico.

À minha família, em especial, ao meu irmão e à minha mãe, obrigada por todo o apoio que deram durante todo o meu percurso académico e por me terem sempre incentivado e por terem estado sempre do meu lado, especialmente quando nem tudo estava a correr bem.

Aos meus amigos, pelos momentos de descontração no meio dos momentos de trabalho, não só durante este ano mas durante todas épocas de exames e meses cheios de trabalhos que passámos juntos. Em especial, à Maria por partilhar comigo as longas horas de trabalho e à minha família de praxe pelos cafés e pelos momentos de desabafo.

Finalmente, quero agradecer ao BEST e ao IEEE por todas as pessoas que conheci, pelos jantares, por todos os momentos bons e menos bons e por me fazerem sair da minha zona de conforto.

"The most beautiful thing we can experience is the mysterious. It is the source of all true art and science."

Albert Einstein

Resumo

A doença vascular periférica afeta entre 3 e 10% da população portuguesa e carateriza-se pelo bloqueio, total ou parcial, dos vasos sanguíneos. Uma das maiores dificuldades associadas a esta doença é distinguir entre os pacientes com maior risco, principalmente nos casos em que estes são assintomáticos. Ao estudar a interação entre eritrócitos em diferentes concentrações de fibrinogénio (uma proteína presente no plasma sanguíneo que promove a adesão entre eritrócitos) é possível estabelecer novos métodos de identificação dos pacientes com maior risco ainda nas fases iniciais da doença. Uma forma de estudar a adesão entre eritrócitos é através da técnica de aspiração por micropipeta. Durante a experiência, cada eritrócito está acoplado a uma micropipeta e, enquanto uma permanece estática, a outra move-se linearmente até que os eritrócitos entrem em contacto, com uma certa força. Depois, a mesma micropipeta, move-se no sentido oposto até que os eritrócitos se separem. Um modelo de simulação matemático da técnica de aspiração por micropipeta foi implementado com o objetivo de fornecer uma ferramenta para quantificar a adesão célula-célula a partir da deformação celular observada durante a sua separação. Esta simulação foi efetuada usando um modelo de campo de fase. Numa primeira fase, foram simulados ambos os eritrócitos, seguida da simulação de ambas as micropipetas e, finalmente, foi adicionada velocidade à micropipeta não estática. Esta simulação permite estudar a adesão entre dois eritrócitos e como diferentes valores de adesão se relacionam com a deformação celular. Eventualmente esta ferramenta poderá levar à criação de melhores métodos quantitativos para medir a adesão dos eritrócitos em pacientes com doenças vasculares.

Palavras-Chave: Modelos de campo de fase, adesão celular, deformação da membrana, modelação matemática, fibrinogénio, eritrócito

Abstract

Peripheral vascular disease affects between 3 and 10% of the Portuguese population and is characterized by total or partial blockage of the blood vessels. One of the biggest difficulties regarding this disease is being able to distinguish which patients are at a higher risk, especially in cases where they are asymptomatic. By studying the interaction between erythrocytes in different concentrations of fibrinogen (a protein present in blood plasma that promotes erythrocyte adhesion) it is possible to establish new methods to identify which patients are at higher risk in the earlier stages of the disease. One way to study the adhesion between two erythrocytes is through the micropipette aspiration assay. During the micropipette aspiration assay, each erythrocyte is attached to a micropipette and, while one of them remains static, the other moves linearly until the erythrocytes are in contact with a certain contact force. Afterwards, the same micropipette moves backward until the erythrocytes separate from each other. A simulation of this micropipette aspiration assay was implemented with the aim of providing a tool to quantify cell-cell adhesion from the observed cell deformation during cell separation. This simulation was done through a phase-field model. Firstly, the shapes of both erythrocytes were simulated, followed by the simulation of the micropipettes, and finally, the velocity was added to the non-static micropipette. This simulation allows to study the adhesion between two erythrocytes and how different values of adhesion are related to cell deformation. Eventually, this tool can create better quantitative methods to measure erythrocyte adhesion in peripheral vascular disease patients.

Keywords: Phase-field models, cell adhesion, membrane deformation, mathematical modeling, fibrinogen, erythrocyte

Contents

List of Abbreviations

Re	Reynolds number.
AFM	Atomic force microscopy.
CAD	Carotid artery disease.
CEA	Carotid endarterectomy.
CFD	Computational fluid dynamics.
CFT	Continuous Fourier Transform.
CVD	Cardiovascular disease.
DFT	Discrete Fourier Transform.
DVT	Deep vein thrombosis.
ECG	Electrocardiogram.
FFT	Fast Fourier Transform.
PAD	Peripheral artery disease.
PE	Pulmonary embolism.
PVD	Peripheral vascular disease.
VTE	Venous Thromboembolism.

List of Tables

List of Figures

1

Introduction

1.1 Motivation

Peripheral vascular disease (PVD) currently affects between 3 to 10% of the Portuguese population, however, these numbers are increasing due to other conditions such as obesity, diabetes, or an aging population [1]. PVD can be defined as an abnormal condition of the blood vessels, where they become completely or partially blocked and can be caused by inflammation, weakness of the vessels or formation of atherosclerotic plaque. Vascular diseases can also affect the heart, brain, or peripheral circulation, which can lead to further complications such as deep vein thrombosis (DVT), peripheral artery disease (PAD), or pulmonary embolism (PE). Atherosclerotic plaques can cause stenosis, embolization, and thrombosis and have been associated with increased concentrations of fibrinogen, a blood protein that increases erythrocyte aggregation. For its role in increasing erythrocyte aggregation, fibrinogen has been studied as a candidate biomarker for the risk of thrombotic events.

One of the major difficulties found in properly treating patients with PVD is the inability to identify those who are at higher risk, especially if the patient is asymptomatic. Currently, the most common non-invasive tests include electrocardiogram (ECG), chest radiography, and transthoracic Doppler-2D echocardiogram. However, none of these tests can detect changes at a cell or molecular levels, and since not all patients can undergo preventive surgery, new biomarkers have been studied to better select which patients need preventive treatment.

By studying the interactions between erythrocytes in different concentrations of fibrinogen, it may be possible to establish new methods to identify the patients at higher risk and at an earlier stage of the disease, using a minimally invasive approach. This can be especially beneficial for asymptomatic patients and for those with a higher chance of recurrence of carotid artery disease (CAD), since it is not always possible to have a consensus regarding treatment guidelines using the diagnostic

tools currently available [2].

1.2 Main goal

The main goal of this master's thesis is to develop a mathematical model able to simulate erythrocyte shape as a function of the force applied, the adhesion between the two cells, and the mechanical characteristics of the cell membrane in the context of a micropipette aspiration assay. This model should also be run to create a database of simulations that can be used to infer the adhesion strength between erythrocytes from the observed alteration of cell morphology in the micropipette assay. This model can also be applied to simulate the interaction between erythrocytes in the presence of different concentrations of fibrinogen.

1.3 Structure

This thesis is divided into 6 main chapters: in chapter 2 is a brief overview of what vascular diseases are, how the concentration of fibrinogen can lead to changes in the adhesion between erythrocytes and, consequently, influence patients with vascular diseases. In chapter 3 is described the mathematical model used to create the simulation model developed through this thesis. In chapter 4 it is presented a detailed description of this simulation model. The results obtained after applying the model are presented in chapter 5 and the conclusions in chapter 6.

2

Background

2.1 Vascular Diseases

Vascular disease is a broad definition that includes any condition that affects the circulation in blood vessels, which means that covers diseases from arteries, veins, and lymph vessels but also includes blood disorders that affect circulation [1]. These conditions may affect other organs such as the brain, heart (cardiovascular diseases, CVD), or peripheral blood vessels.

Peripheral vascular disease (or peripheral artery disease, if the vessel affected, is a peripheral artery) is an abnormal condition where the blood vessels are partially or completely blocked, as is illustrated in figure 2.1. This may happen due to an inflammatory process, vessel weakness, or the formation of atherosclerotic plaque [3]. Atherosclerotic plaque consists in the buildup of fat and cholesterol deposits inside the blood vessels, which will reduce the thickness of the blood vessels reducing the blood flow to the tissues. In addition to aggravating complications of peripheral blood circulation, atherosclerosis can cause stenosis, embolization, and thrombosis [4]. It was also associated with high levels of fibrinogen, which result in changes in rheology [3].

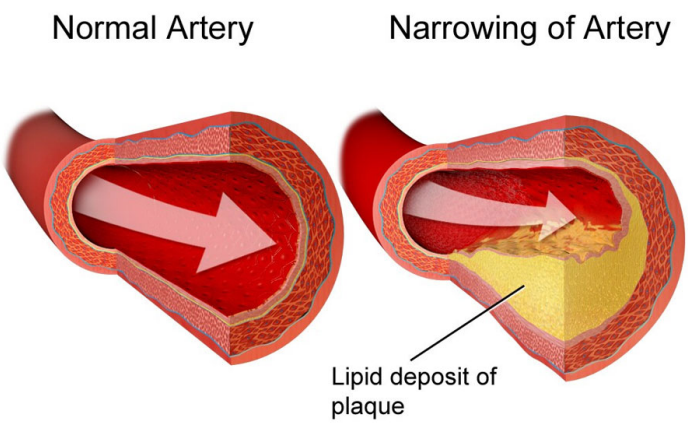

Figure 2.1: Difference between a healthy artery and a partially blocked artery with the formation of the atherosclerotic plaque, adapted from [5]

When the atherosclerotic plaques are formed in the carotid artery the condition is called Carotid Artery Disease (CAD) and the patients can be symptomatic or asymptomatic. Another common vascular disease is deep vein thrombosis (DVT), which occurs when a blood clot forms in a deep vein. This condition can also lead to chronic obstructive lesions, deep vein valvular insufficiency, or the development of a pulmonary embolism (PE). When both DVT and PE conditions exist simultaneously can be called venous thromboembolism (VTE) [6]. The recurrence risk of DVT, especially if non-provoked or idiopathic, can be up to 20% at 2 years. Also, it is not always easy to select patients who need preventive surgery for CAD so, it is necessary to find new biomarkers that allow to better understand the mechanisms underlying both conditions and, in this way, improve the patient's clinical diagnosis and prognosis.

2.2 Erythrocytes

Erythrocytes, figure 2.2, also known as red blood cells, are an essential component of the blood responsible for carrying oxygen from the lungs to the various cells and tissues and removing carbon dioxide from those tissues. Erythrocytes are biconcave cells filled with hemoglobin that allows them to carry more oxygen to the cells and squeeze through narrow blood vessels to reach them. Erythrocytes are produced in the bone marrow and their typical lifespan is 120 days, after which they are removed from circulation and broken down in the spleen and liver.

When the concentration of erythrocytes in the blood is different from its typical value it can lead to health complications: If the erythrocytes concentration is too low

can lead to anemia, which causes symptoms like fatigue and weakness. An excessive number of erythrocytes can lead to problems related to blood flow and clotting [7].

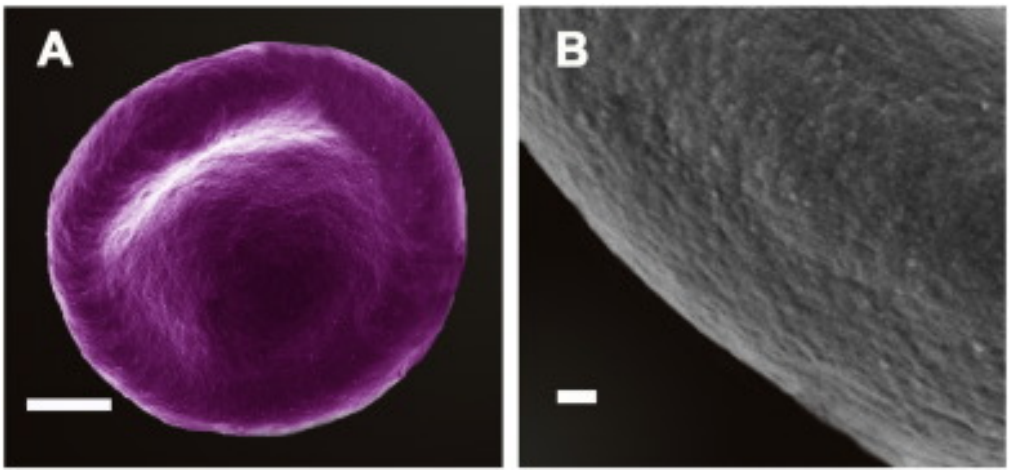

Figure 2.2: Microscopic image of A)healthy erythrocyte; B) high magnification of the erythrocyte membrane. Scale bar: A) 1 μm; B) 100nm. Adapted from [7]

Alterations in the molecular arrangement of erythrocyte membrane biophysical properties may lead to changes in the overall shape of the cell, including altered membrane elasticity/rigidity. These alterations could cause different structural cell deformability and changes in blood rheology, which may be the consequence of inflammatory pathophysiologies in the vascular system [7, 8].

Erythrocyte-erythrocyte adhesion is essential to blood clotting in wound healing, where it is initially mediated by platelets and then by a fibrin mesh. Sometimes blood clots, or thrombi, form inside blood vessels, both in arteries or veins or in the heart, and can lead to blood flow complications. The formation of thrombi in the peripheral blood circulation is dependent on the concentration of fibrinogen [9]. Fibrinogen is one of the blood's most abundant plasma proteins and plays a role in the coagulation process being a key factor in forming blood clots by polymerizing in a fibrin network and entrapping blood cells. Fibrinogen level is a marker of inflammation and could give information about clotting disorders or the risk of developing cardiovascular diseases. Elevated concentrations of this protein promote erythrocyte aggregation and are a good candidate to be a biomarker for thromboembolic events [7, 10]. The presence of fibrinogen in atherosclerotic plaques indicate that it plays a role in their development and stability. With the use of atomic force microscopy (AFM)-based force spectroscopy, it was possible to demonstrate the specific receptor for fibrinogen in the erythrocyte membrane (will be explained in section 2.5). The binding of this receptor by a fibrinogen molecule simultaneously on two different erythrocytes may bridge these cells increasing their adhesion and

leading to an increased blood viscosity and of vascular risk.

The adhesion between erythrocytes has been measured using different techniques such as AFM or micropipette aspiration for different concentrations of fibrinogen [8].

2.3 Fibrinogen

Fibrinogen is a 340kDa glycoprotein comprised of two symmetric half molecules, each comprised of one set of three polypeptide chains: $A\alpha$, $B\beta$ and γ (figure 2.3). Fibrinogen has three potential integrins (transmembrane receptors that facilitated cell-cell and cell-extracellular matrix adhesion) binding sites, one of which can also interact with cells through nonintegrin receptors. The membrane glycoprotein complex $a_{IIb}\beta_3$ is the platelets integrin receptor for fibrinogen [11].

Fibrinogen is synthesized by hepatocytes, which are cells in the liver and circulates as a blood component with a concentration of approximately 2-4 g/L [12] and a half-life of 100 hours, however, the synthesis of fibrinogen is increased during episodes of inflammation [13].

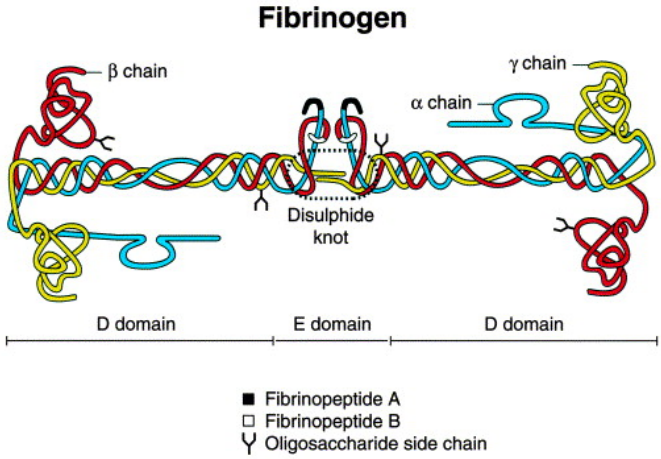

Figure 2.3: Schematic diagram of fibrinogen molecule, adapted from [13]

Fibrinogen plays a role in controlling blood loss and clot formation: it is essential for platelet aggregations and forms an insoluble fibrin clot in the final stage of the blood coagulation cascade [12, 13]. In figure 2.4 it is possible to observe erythrocytes trapped in this fibrin mesh.

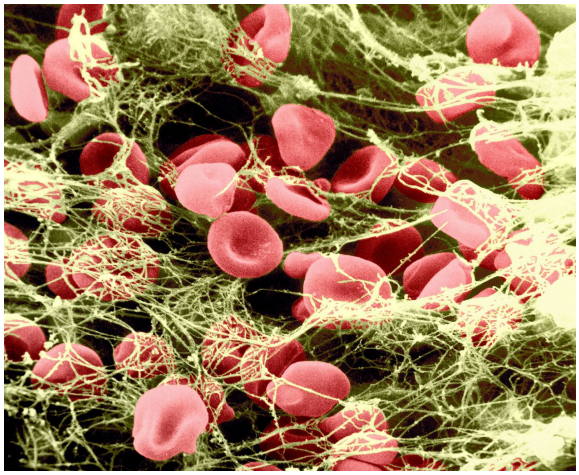

Figure 2.4: Erythrocytes trapped in a fibrin mesh, adapted from [14]

2.4 Fibrinogen and vascular diseases

Fibrinogen is a plasma protein that plays a central role in coagulation and thrombosis by polymerizing in a fibrin network entrapping blood cells [10]. Fibrinogen levels also increase during inflammation, particularly in the case of γ' fibrinogen, a variant of fibrinogen with 20 amino acids extension on the γ chain that constitutes 7% of total plasma fibrinogen. γ' fibrinogen has different biochemical and biophysical properties that contribute to the thrombosis [10, 15]. Studies also show an increased risk of PE in patients with higher concentrations of plasma fibrinogen [16].

In the case of VTE, it is known that it is triggered by inflammation and blood stasis leading to the formation of thrombi rich in fibrin and erythrocytes. Because of this, fibrinogen can also be a determinant of VTE risk [6].

In the case of atherosclerosis, there is fibrin accumulation within the atherosclerotic plaque, especially in the late stages of plaque formation. Since an increased concentration of fibrinogen is key determinant of fibrin formation it is also a risk factor for atherosclerotic vascular diseases, namely, coronary artery stenosis and myocardial infarction [4].

Fibrinogen can be considered a good biomarker for the risk of thromboembolic events. Thus studying its interaction with erythrocytes may help identify the patients that are at higher risk on an earlier stage of the disease in conditions like DVT and CAD [16].

By studying the erythrocyte deformability it has been possible to conclude that CAD patients who underwent a carotid endarterectomy (CEA) had reduced erythrocyte deformability before the surgery, which was not observed 6 months

after it. By total plasma fibrinogen quantification was also possible to observe that these patients had higher values before surgery than the control group and had an increased erythrocyte stiffness.

By looking at these studies it was possible to conclude that the interactions between erythrocytes and fibrinogen play a crucial role in multiple diseases since they impact erythrocyte stiffness and adhesion, leading to changes in local hemodynamic flow, and are essential to the formation of atherosclerotic lesions.

2.5 Atomic Force Microscopy

AFM is a scanning imaging and manipulation technique used in different fields of research that allows the study of surfaces and structures at the nanoscale with high resolution and precision [17]. Particularly in medicine, AFM can be used in research and diagnostics by providing information at a nanoscale level that can then be used in the development of new medical technologies and therapies [17].

AFM works by scanning a cantilever with a sharp tip at the end, across the surface of the sample to be analyzed. The forces that result from the interaction between the sample and the tip can then be measured and used to create an image of the surface topography. The forces measured can also be used to study the mechanical properties of the sample, such as elasticity and protein-cell receptor interaction [9, 17].

AFM is a technology that allows cell elasticity and surface roughness. Since one of the characteristics of healthy erythrocytes is their ability to return to their original form after being deformed, this technique allows us to determine changes in cell elasticity [7]. To study the adhesion between erythrocytes using AFM, one erythrocyte was attached to the cantilever while the other was adhered to the surface, which allowed to collect the force-distance curves for cell-cell adhesion at different concentrations of fibrinogen [8].

The fibrinogen-induced erythrocyte aggregation has been considered to be caused by a single molecule interaction between the fibrinogen and a receptor on the erythrocyte's membrane [9].

AFM was used to study the specific binding between fibrinogen and the receptor in the erythrocyte membrane, while also making an equivalent study using platelets to compare the results [11]. The results obtained indicated that the specific binding between the erythrocyte and the fibrinogen has a comparable affinity to the platelets binding and that the interaction was mediated by an integrin $a_{IIb}\beta_3$-like receptor [11]. Further studies allowed to conclude that the receptor for fibrinogen

in erythrocytes is the $a_v\beta_3$ integrin, by measuring the inhibition of the fibrinogen-erythrocyte interaction by specific antibodies against a_v and $a_v\beta_3$ integrins [17].

2.6 Micropipette aspiration assay

Micropipette aspiration is a technique used to measure the mechanical properties of cells at a microscopy level, such as cell elasticity and membrane tension [8].

This technique uses a micron-sized pipette, usually a glass capillary with a fine tapered tip, to aspirate a small portion of the cell into the micropipette itself under controlled suction forces. These forces can be maintained throughout the assay.

To measure the adhesion between two erythrocytes, a technique with two micropipettes was used, which allowed to observe alterations in the erythrocytes shapes as they come into contact [8]. During this experiment, a linear translator coupled to one of the micropipettes allowed to control the movements of approach, adhesion, and retraction between the erythrocytes. This system is also able to acquire real-time video images.

The schematic experimental setup representation can be found in the figure 2.5. One of the micropipettes, in this case, the one on the left, is kept static, while the other micropipette, with an erythrocyte attached, approach to the erythrocyte attached to the static micropipette until a certain contact force is reached. During the retraction of the piezo-driven micropipette, cell-cell adhesion may occur, which leads to the pulling of the surface of the erythrocyte from the left side, until there is a complete detachament of both erythrocytes [8].

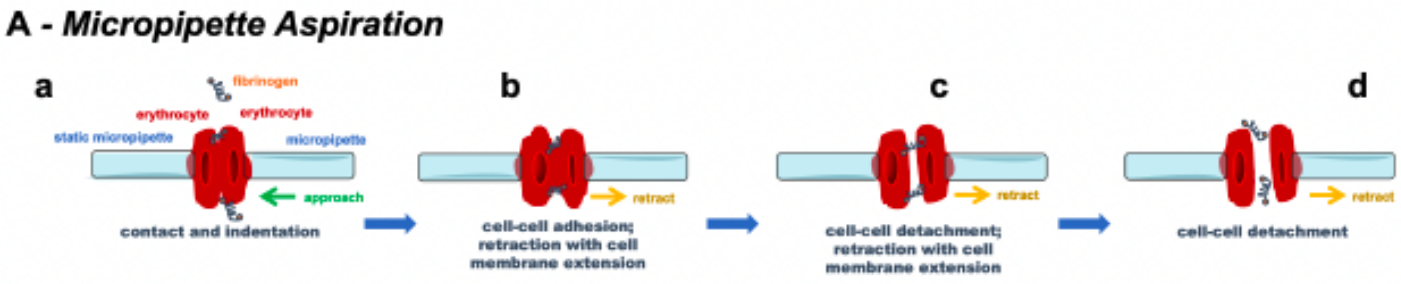

Figure 2.5: Schematic experimental setup representation of the micropipette aspiration assay, adapted from [8]

From the micropipette aspiration assay, it is possible to capture video images of the interaction between two erythrocytes. Figure 2.6 shows some microscopic

images captured during the experiment, with and without the addition of fibrinogen at 1mg/mL of concentration.

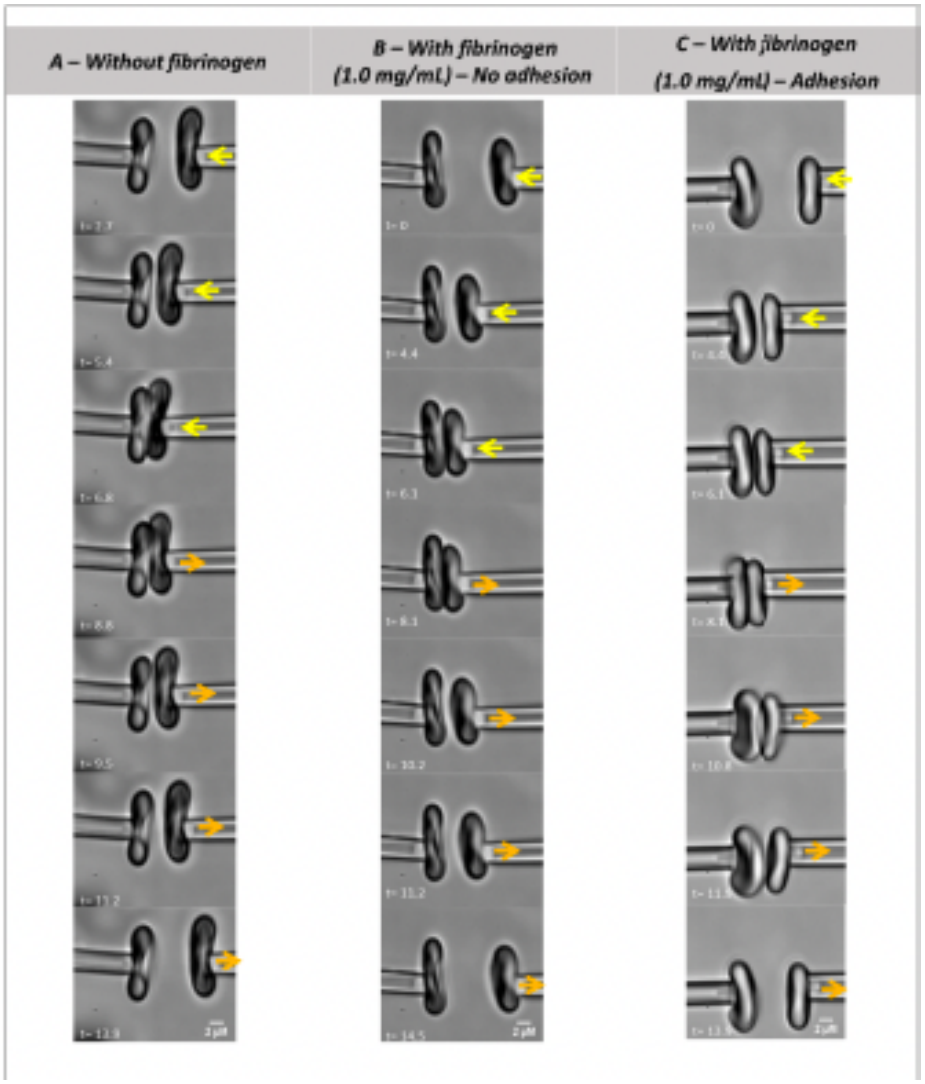

Figure 2.6: Sequence of microscopy images at different stages of the erythrocytes-erythrocyte adhesion with and without the presence of fibrinogen. Adapted from [8]

Micropipette aspiration measures the degree of membrane deformation, which allows the estimation of the cell stiffness, in response to a negative pressure applied to the cell surface. This technique was also used to determine the elastic properties of erythrocytes as a function of temperature [7].

3

Phase-field model and mathematical tools

3.1 Phase-field model

Cell membranes act as a boundary between internal cellular organization and the surrounding medium and are composed of several kinds of lipids, namely phospholipids, cholesterol, and glycolipids, which are assembled in a fluid bilayer, and proteins [18]. Even though biological membranes are complex structures, there are some universal common principles, such as the presence of a fluid lipid bilayer and proteins that can diffuse on the surface of the membrane.

One of the mathematical tools used to study complex interfacial problems is a phase-field model also known as diffuse interface model [18]. Phase-field models disregard microscopic details of the systems, describing the dynamics of the closed interfaces as a function of their surface tension or bending energies. A biological membrane can be considered a mathematical interface between two phases: the inner fluid and the outer fluid. However, during the evolution of a cellular membrane, some geometrical constraints should be considered and thus implemented in the phase-field model: the conservation of the membrane area (disregarding events of endocytosis and exocytosis) and the conservation of the cell volume (disregarding the osmotic transport of water).

3.1.1 Canham-Helfrich free energy

One of the free energy functionals used to describe lipid bilayer membranes is the *Canham-Helfrich* free energy, which is applied to liquid membranes governed by bending energy [19]. This free energy involves the mean and Gaussian curvatures of the mid-surface of the lipid bilayer and the local bending energy is an expansion in terms of these invariants [20]. If the membrane has an asymmetry between the two layers, the membrane can present a spontaneous curvature and the free

energy density is given by the equation 3.1, where κ and κ_G are elastic constants corresponding to the bending rigidity and the Gaussian bending rigidity. The term K is the Gaussian curvature term and, when integrated over a closed surface is topological invariant and thus can be considered a constant factor since the focus of the work will not be to study topological changes [18].

$$f_{C-H,sc} = \frac{\kappa}{2}(2H - c_0)^2 + \kappa_G K \tag{3.1}$$

After integration over the whole membrane surface the membrane free energy is given by the equation 3.2, where Γ is the membrane surface. The specific case where $c_o = 0$ is the minimal model, where there is no asymmetry between the lipidic layers of the membrane [18].

$$f_{C-H,sc} = \frac{\kappa}{2}\int_{\Gamma}(2H - c_0)^2 ds \tag{3.2}$$

3.1.2 Minimal model

To obtain a phase-field model it is necessary to write the free energy functional, as a function of an order parameter, ϕ, that identifies the cell. This free energy functional will be equivalent to the equation 3.2 when $c_o = 0$.

$$F[\phi] = \int_{\Omega} \Phi^2[\phi] dx \tag{3.3}$$

The function Φ depends on the order parameter ϕ and is defined by the equation 3.4, where ϵ is a small parameter related to the interface width.

$$\Phi[\phi(x)] = -\phi + \phi^3 - \epsilon^2 \nabla^2 \phi(x) \tag{3.4}$$

The implementation of this model can be used to achieve the stationary shapes (figure 3.1) of cells such as erythrocytes. These shapes are achieved by starting from an initial arbitrary shape corresponding to the value of the reduced volume and the initial condition of the phase-field is a sharp distribution of $\phi = +1$ inside the cell and ϕ = -1 outside the cell (although some works may use $\phi = +1$ inside the cell and $\phi = 0$ outside the cell) [8, 18].

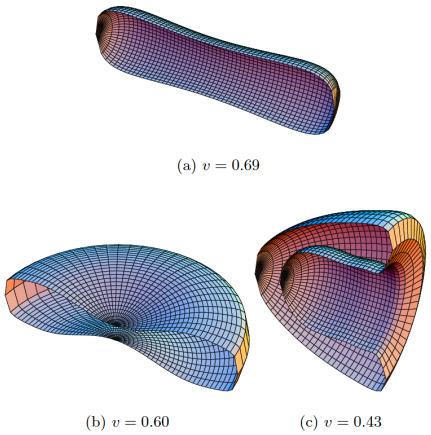

(a) $v = 0.69$

(b) $v = 0.60$ (c) $v = 0.43$

Figure 3.1: Stationary shapes as stationary states of the dynamic evolution of certain initial conditions. a) prolate, b)oblate, c) stomatocyte. Adapted from [18]

3.2 Erythrocyte phase-field model

In the mathematical model used to describe the erythrocytes a scalar order parameter was assigned to each erythrocyte, $\phi_i(\vec{r})$, where i identifies the cell. This parameter can be defined as $\phi_i \approx +1$ inside the respective erythrocyte and $\phi_i \approx -1$ outside, near the membrane it varies continuously, and $\phi_i = 0$ in the center of the interface. The free energy of a group of cells would be given by a sum of terms equal to the free energy functional of equation 3.3 for each cell.

However, when studying the erythrocytes' shapes and dynamics, there are several energies involved, such as the bending energy due to the curvature, the adhesion energy between the two erythrocytes, and the hard-core repulsion that prevents inter-penetration between the two erythrocytes. In this way, the free energy of the two cell system is given by equation 3.5.

$$\begin{aligned} F[\phi_1(\vec{r}),\phi_2(\vec{r})] = & \int \kappa_B \sum_{i=1}^{2} (-\phi_i + \phi_i^3 - \epsilon^2 \nabla^2 \phi_i)^2 d\vec{r} \\ & + \int (\gamma h(\phi_1) h(\phi_2) + \eta \nabla h(\phi_1) \cdot \nabla h(\phi_2)) d\vec{r} \\ & + \alpha_S \sum_{i=1}^{2} (S_{target} - S[\phi_i])^2 \\ & + \alpha_V \sum_{i=1}^{2} (V_{target} - V[\phi_i])^2 \end{aligned} \tag{3.5}$$

The free energy function that was implemented, equation 3.5, takes into account different energetic contributions, such as the rigidity of the membrane (first term of the equation), the hard-core repulsion of the erythrocytes, the cell-cell surface adhesion and the conservation of the volume and of the surface area. γ is a coefficient proportional to the hard-core repulsion between the erythrocytes while η is proportional to the cell-cell surface adhesion. The function h, equation 3.6, is approximately $\frac{1}{2}$ at the vicinity of $\phi_i = 0$ and it is $h(-1) = 0$ and $h(1) = 1$. This function moderates the hard-core repulsion term that otherwise would push the order parameter values outside of the interval [−1,1] [8].

$$h(\phi_i) = \frac{1}{4}(1+\phi_i)^2(2-\phi_i) \tag{3.6}$$

From the free energy (equation 3.5) it is possible to calculate the equation for the time evolution of the order parameter. The equation 3.7 shows for the order parameter ϕ_1, the equation that accounts for the other erythrocyte, which can be obtained by exchanging the indices 1 and 2. $\vec{v}$ is the advection velocity of the cell and M is the system's mobility. The model parameters can be found in table 3.1.

$$\begin{aligned}
\frac{\partial\phi_1}{\partial t} + \vec{v}\cdot\nabla\phi_1 = -M\frac{\delta F}{\delta\phi_1} = \\
&- M[2(3\phi_1^2-1)\kappa_B(-\phi_1+\phi_1^3-\epsilon^2\nabla^2\phi_1) \\
&- 2\kappa_B\epsilon^2\nabla^2(-\phi_1+\phi_1^3-\epsilon^2\nabla^2\phi_1) \\
&+ \frac{3}{4}\gamma(1-\phi_1^2)h(\phi_2) - \frac{3}{4}\eta(1-\phi_1^2)\nabla^2 h(\phi_2)] \\
&- 3\sqrt{2}M\epsilon\alpha_S(S_{target}-S[\phi_1])\nabla^2\phi_1 \\
&+ \frac{3}{2}M\alpha_V(V_{target}-V[\phi_1])(1-\phi_1^2)
\end{aligned} \tag{3.7}$$

Table 3.1: Model parameters, adapted from [8]

Parameter	Symbol	Value	Units
Bending rigidity coefficient	k_B	432	J/m^3
Interface width	ϵ	0.17	μm
Hard-core repulsion coefficient	γ	138	J/m^3
Area conservation coefficient	α_S	1.8×10^{-2}	J/mm^4
Volume conservation coefficient	α_V	5.9×10^4	J/mm^6
Target area	S_{target}	197	μm^2
Target volume	V_{target}	160	μm^3
Mobility	M	7.4×10^{-2}	$m^3 J^{-1} s^{-1}$
Velocity	$\|\|\vec{v}\|\|$	0.57	μ m/s

The force of the interaction of one erythrocyte with the other erythrocyte can be calculated by equation 3.8 [8].

$$\begin{aligned} \vec{F_1} &= -\int \phi_1 \nabla \frac{\delta F_{interation}}{\delta \phi_1} d\vec{r} = \\ &= -\int \frac{3}{4}\phi_1 \nabla(\gamma(1-\phi_1^2)h(\phi_2) - \eta(1-\phi_1^2)\nabla^2 h(\phi_2))d\vec{r} \end{aligned} \tag{3.8}$$

The shape of each cell was obtained from the integration of the equation 3.7, with the velocity and cell-cell interaction terms set to zero. The initial ellipsoid shape and the final shape of the erythrocytes can be found on figure 3.2.

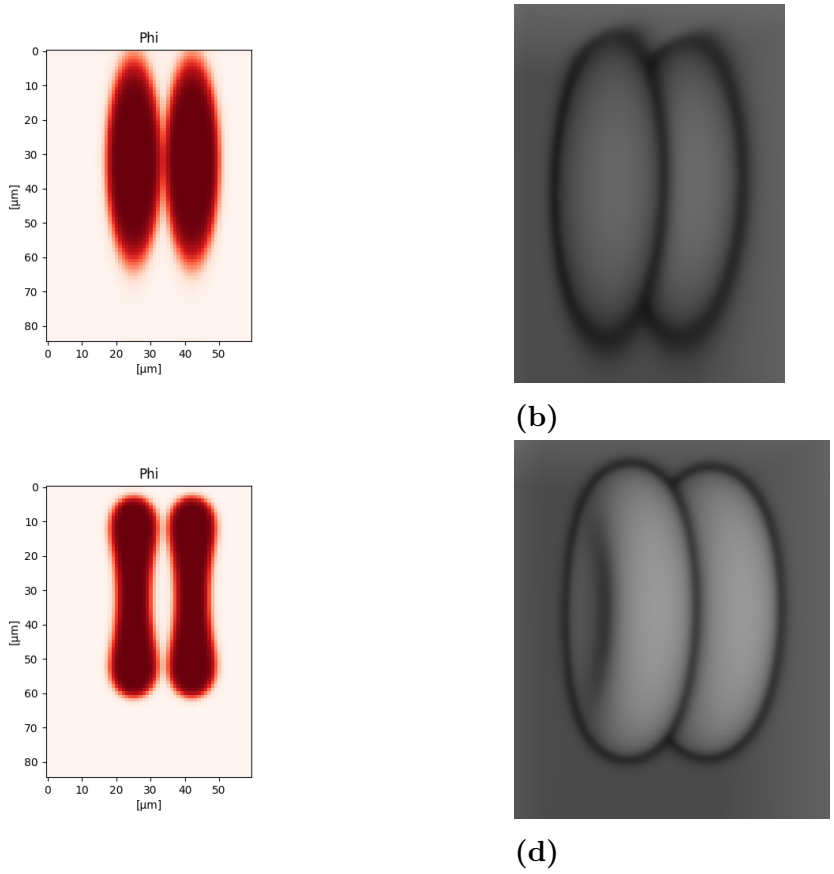

(a) **(b)**

(c) **(d)**

Figure 3.2: Example of initial conditions and final shape of the erythrocytes. The possible initial conditions are shown in figures (a) and (b), where figure (a) is a mid-slice profile of the same conditions shown in figure (b). The final shape of the erythrocytes is shown in figures (c) and (d), where (c) is a mid-slice profile of the erythrocytes shown in figure (d)

3.3 Navier-Stokes equations

The Navier-Stokes equations are a set of nonlinear partial differential equations that describe the behavior of fluid flow, more specifically the conservation of momentum for a fluid [21]. These equations are in vector form and can be written for incompressible flow, where fluid density is constant, or for compressible flow, where fluid density can vary. These equations describe how fluid velocity and pressure change over time due to several factors, such as pressure gradients and external forces [21].

In the case of incompressible flow, the Navier-Stokes are usually written as a continuity equation (equation 3.9) and a momentum equation (equation 3.10) [21]. The continuity equation represents the conservation of mass and states that the divergence of the velocity v (also in vector form) is zero and the momentum

equation describes the conservation of momentum. The meaning of each variable of both equations is in the table 3.2.

$$\nabla \cdot \vec{v} = 0 \tag{3.9}$$

$$\rho(\frac{\partial \vec{v}}{\partial t} + (\vec{v} \cdot \nabla)\vec{v}) = -\nabla p + \mu \nabla^2 \vec{v} + \vec{F} \tag{3.10}$$

Table 3.2: Variables of the Navier-Stokes equations

Symbol	Meaning
$\frac{\partial \vec{v}}{\partial t}$	Variability rate of the velocity in order of time
$\vec{v}$	Velocity vector
∇	Gradient
p	Pressure
ρ	Fluid density
μ	Dynamic viscosity of the fluid
$\nabla^2 \vec{v}$	Laplacian of the velocity
$\vec{F}$	External forces acting on the fluid

Since these equations are nonlinear partial differential equations their complete analytical solution is only possible for simple cases. In more complex situations it is necessary to use other numerical methods such as computational fluid dynamics (CFD) [21].

3.3.1 Reynolds number

The Reynolds number, Re, is a dimensionless quantity (described in equation 3.11) that characterizes the relative importance of inertial forces to viscous forces. It is used in fluid mechanics to predict the flow regime of a fluid around an object or inside a pipe. In equation 3.11, ρ represents the fluid density, V the characteristic fluid velocity, μ the fluid dynamic viscosity and L is a characteristic length, like the diameter of a pipe or the length of an object.

$$Re = \frac{\rho V L}{\mu} \tag{3.11}$$

The Reynolds number helps to determine whether the flow is laminar, transitional, or turbulent, which can have a significant impact on several aspects of

fluid behavior, such as drag forces and heat transfer. The Reynolds number range corresponding to each flow regime can be found in table 3.3 [22].

Table 3.3: Reynolds number and corresponding flow regime

Reynolds number range	Flow regime	Characteristics of the flow
$Re < 2000$	Laminar flow	Smooth and predictable, characterized by steady and well-defined streamlines, with fluid particles moving in parallel layers. Viscous forces dominate.
$2000 < Re < 4000$	Transitional flow	The flow is transitioning between laminar and turbulent. It can become unpredictable due to the appearance of the turbulence.
$Re > 4000$	Turbulent flow	The flow is turbulent and chaotic, characterized by irregular and mixing motion of fluid particles. As the Reynolds number increases so does the turbulence.

3.3.2 Reynolds number and the Navier-Stokes equations

The Reynolds number is closely related to the Navier-Stokes equations since it describes the flow regime that these equations describe and thus can influence how fluid behavior is modeled, functioning as a bridge between the characteristics of the flow and the mathematical equations [22].

The relation between the Reynolds number and the Navier-Stokes equations can be mainly summarized in two points: flow regime determination and modeling approach. Relatively to the flow regime determination, the Reynolds number helps to determine the flow regime for a specific situation: in the case of laminar flow the nonlinear convective terms of the Navier-Stokes $((\vec{v} \cdot \nabla)\vec{v})$ are less significant and the equation can be simplified. Relatively to the modeling approach the Reynolds number can help guide the choice of modeling approach when solving fluid flow problems: for low Re, which describes a laminar flow, and the Navier-Stokes equations can be simplified it is possible to use analytical solutions and simpler numerical techniques. However, for higher Reynolds numbers and turbulent flows,

it is necessary more complex and advanced numerical methods in order to solve the complete Navier-Stokes equations [23].

3.4 Fourier Transform

The Fourier Transform is a mathematical tool used in several fields that allows the decomposition of a function into its constituent frequencies, by equivalently representing a periodic signal in sinusoids that are harmonically related to the base frequency of the signal. The Fourier Transform is one of the most general ways to analyze the frequency characteristics of a signal since it makes the fewest assumptions about it [24].

The Fourier Transform is an operation that transforms data from the time or spatial domain into the frequency domain. The continuous Fourier Transform (CFT) is defined for continuous functions (equation 3.12), where $F(\omega)$ is the Fourier Transform of the function $f(t)$ and is function of the angular frequency ω [25, 26].

$$F(\omega) = \int_{-\infty}^{\infty} f(t) \cdot e^{-i\omega t} dt \tag{3.12}$$

The function $F(\omega)$ is a complex-valued function of ω that represents the contribution of each frequency component to the original function, $f(t)$.

In the case of discrete functions, the discrete Fourier Transform (DFT) is used instead, a finite version of the continuous Fourier Transform, and it is commonly computed by the Fast Fourier Transform (FFT) algorithm [26].

The inverse Fourier Transform (equation 3.13) allows the reconstruction of the original function $f(t)$ from its frequency domain representation, $F(\omega)$ [26].

$$f(t) = \frac{1}{2\pi} \int_{-\infty}^{\infty} F(\omega) \cdot e^{i\omega t} d\omega \tag{3.13}$$

3.4.1 Fast Fourier Transform

The Fast Fourier Transform (FFT) is an efficient algorithm used to compute the DFT of a sequence (which is a finite set of discrete data points sampled from a continuous signal). This algorithm can speed up the computation of the DFT, which makes it practical for real-time applications and large datasets. This speed-up is due to a difference in the computational complexity since most FFT algorithms have a number of operations on the order of $O(N\log N)$, where N is the number of data points and the direct computation of the DTF has a number of operations on the

order of $O(N^2)$, making it slower for larger values of N. However, the efficiency of the FFT algorithm depends on the choice of the FFT variant and on the properties of the input data [27, 28].

The FFT algorithm is based on a "divide and conquer" approach, which means that it recursively breaks down the DFT into smaller DFTs, exploiting the periodicity and symmetry properties of complex exponentials to reduce the number of computations.

The FFT can also be used to compute the inverse Fourier Transform of a function, allowing it to convert the data back from the frequency domain to the time domain.

4

Numerical Implementation

As stated in section 1.2, the main goal of this simulation is to model and predict the erythrocyte shape as a function of the force applied and the adhesion between the two erythrocytes in the context of a micropipette aspiration assay.

In order to achieve this objective the simulation model was made in three different sections: first, it was necessary to create the shapes of the erythrocytes, then the two micropipettes were designed, and finally, the velocity was added to one of the micropipettes, since the other remains static [8].

4.1 Erythrocytes model

The phase-field model used to create the 3D shape of both erythrocytes was based on the model described in section 3.2, more specifically, in equation 3.7, having as the starting point an ellipsoid shape.

This model also uses a scalar order parameter to describe each of the erythrocytes, ϕ_i, where i identifies each of the erythrocytes, that will be defined as $\phi_1 \approx +1$ inside the cell and $\phi_i \approx -1$ outside the cell, near the membrane varying within the interval $[-1, +1]$, being $\phi_i \approx 0$ near the center of the interface.

Even though the simulation is based on equation 3.7 the terms that describe the interaction between two erythrocytes, both repulsion and adhesion, and the velocity term are absent. The equation without these terms is equation 4.1, where S_{ϕ_i} and V_{ϕ_i} are the surface area and the volume of the erythrocyte, respectively.

$$\begin{aligned}\frac{\partial \phi_i}{\partial t} =& -2Mk_b(3\phi_i^2 - 1)(-\phi_i + \phi_i^3 - \epsilon^2\nabla^2\phi_i) \\ & - 3\sqrt{2}M\epsilon\alpha_S(S_{target} - S_{\phi_i})\nabla^2\phi_i \\ & + \frac{3}{2}M\alpha_V(V_{target} - V_{\phi_i})(1 - \phi_i^2) \\ & + 2Mk_B\epsilon^2\nabla^2(\phi_i^3 - \phi_i - \epsilon^2\nabla^2\phi_i)\end{aligned} \tag{4.1}$$

In table 4.1 there are the initial values for the parameters used in equation 4.1. The area conservation coefficient, α_S, and the target area, S_{target}, are zero for the first iterations, however after those initial iterations, the interface is well formed and $\alpha_S = 1.8 \times 10^{-2}$ (same as in table 3.1). The cell area is calculated using equation 4.2 [8].

Table 4.1: Initial model parameters for the simulation of erythrocytes shapes

Parameter	Symbol	Value	Units
Bending rigidity coefficient	k_B	432	J/m^3
Interface width	ϵ	0.17	μm
Hard-core repulsion coefficient	γ	138	J/m^3
Area conservation coefficient	α_S	0	J/mm^4
Volume conservation coefficient	α_V	5.9×10^2	J/mm^6
Target area	S_{target}	0	μm^2
Target volume	V_{target}	Volume of the initial ellipsoid	μm^3
Mobility	M	7.4×10^{-2}	m$^3 J^{-1} s^{-1}$

The target area is set equal to the cell area calculated by equation 4.2 at the moment α_S is set to a value different from zero.

$$S[\phi_i] = \frac{3}{2\sqrt{2}}\epsilon \int (\nabla\phi(\vec{r}))^2 d\vec{r} \tag{4.2}$$

Even though the non-linear terms of equation 4.1 (the first three terms) were initially calculated in real space, the next iteration of the order parameters was calculated in the Fourier space, using the FFT algorithm.

On the experimental micropipette aspiration assay, the aim is for the erythrocytes to be aligned. This is not always possible and in some experiments, they can be misaligned. Both of these situations can be simulated with this model by defining different coordinates for the center of the initial ellipsoid.

4.2 Velocity

During the micropipette aspiration assay, the velocity is not applied directly to the erythrocytes, as it happens in equation 3.7, but instead, it is applied in the micropipettes. The total velocity can then be decomposed into the velocity of the movement of the micropipette and the fluid velocity (equation 4.3).

$$\vec{v} = \vec{v}_{trans} + \vec{v}_{Navier-Stokes} \tag{4.3}$$

The fluid velocity was based on the Navier-Stokes equations (section 3.3) and the equation used to describe it is equation 4.4, where η is the fluid viscosity.

$$\rho(\partial_t \vec{v} + (\vec{v} \cdot \nabla)\vec{v}) = -\nabla p + \eta \nabla^2 \vec{v} + \vec{F}_{ext} \tag{4.4}$$

The equation 4.4 can be simplified since $\rho(\partial_t \vec{v} + (\vec{v} \cdot \nabla)\vec{v}) \approx 0$, because Re is very small. The external force can be described by the equation 4.5, where $\mu = \frac{\partial F}{\partial \phi_1}$. and it is described by the equation 4.6.

$$\vec{F}_{ext} = \phi_i \nabla \mu \tag{4.5}$$

$$\begin{aligned}
\mu &= 2(3\phi_1^2 - 1)\kappa_B(-\phi_1 + \phi_1^3 - \epsilon^2\nabla^2\phi_1) \\
&- 2\kappa_B\epsilon^2\nabla^2(-\phi_1 + \phi_1^3 - \epsilon^2\nabla^2\phi_1) \\
&+ \frac{3}{4}\gamma(1 - \phi_1^2)h(\phi_2) - \frac{3}{4}\eta(1 - \phi_1^2)\nabla^2 h(\phi_2) \\
&+ 3\sqrt{2}\epsilon\alpha_S(S_{target} - S[\phi_1])\nabla^2\phi_1 \\
&- \frac{3}{2}\alpha_V(V_{target} - V[\phi_1])(1 - \phi_1^2) \\
&+ \frac{3}{4}\gamma_{\pi 1}(1 - \phi_i^2)h(\pi_1) - \frac{3}{4}\gamma_{\pi 2}(1 - \phi_i^2)h(\pi_2)
\end{aligned} \tag{4.6}$$

However, due to a very small Reynolds number, the Navier-Stokes velocity component can be dismissed, so the velocity is solely provided by the pushing and pulling of the micropipette.

4.3 Micropipettes

The micropipettes for both erythrocytes were identically simulated, using two scalar order parameters: π_1 and π_2, where π_1 represents the micropipette wall and π_2 the space in its interior. The equations 4.7 and 4.8 describe their time evolution, respectively, with $\vec{v}_{\pi 1} = \vec{v}_{\pi 2}$ as the translation velocity of the micropipette. However, for one of the erythrocytes, usually represented on the left, the velocity is zero so the velocity terms can be omitted for that micropipette. The other terms of these equations lead to the formation of smooth interfaces of the micropipette to prevent an abrupt change between values.

$$\frac{\partial \pi_1}{\partial t} = \epsilon^2 \nabla^2 \pi_1 + \pi_1 - \pi^3 - v_{\pi_1} \nabla \pi_1 \tag{4.7}$$

$$\frac{\partial \pi_2}{\partial t} = \epsilon^2 \nabla^2 \pi_2 + \pi_2 - \pi^3 - v_{\pi_2} \nabla \pi_2 \tag{4.8}$$

The parameter is $\pi_1 = +1$ inside the micropipette wall and $\pi_1 = -1$ in the rest of the space. To prevent the erythrocyte from going through the micropipette wall a repulsion term (equation 4.9, see also equation 4.6) needs to be added to the equation that describes the evolution of the scalar order parameter for each erythrocyte (equation 3.7). In this term $\gamma_{\pi 1} = 30$ and the function $h(\phi_i) = \frac{1}{4}(1 + \phi_i)^2(2 - \phi_i)$ (equation 3.6).

$$-\frac{3}{4} M \gamma_{\pi 1} (1 - \phi_i^2) h(\pi_1) \tag{4.9}$$

The parameter π_2 represents the space inside the micropipette and its $\pi_2 = +1$ inside that space and $\pi_2 = -1$ outside it.

To simulate the pressure that the micropipette enforces on the erythrocyte, similarly to what was done with π_1, it was necessary to add a new term to the equation of the evolution of the erythrocytes (equation 4.10, see also equation 4.6). The function h is the same as the in equation 3.6. However, the calculation of the term $\gamma_{\pi 2}$ was made in two ways: in the first approach, it was simply computed that $\gamma_{\pi 2} = \textit{constant}$. In a second approach, the value of $\gamma_{\pi 2}$ varies linearly with the distance to the beginning of the micropipette (the place where it is in contact with the erythrocyte). This dependence is in equation 4.11, where $m = 4$, $\gamma_2 = 34$, which was the value with the best results with the first approach, and z_0 is the coordinate of the center of the micropipette along the z axis, which is the axis along which the velocity will be applied to the micropipette.

$$+\frac{3}{4} M \gamma_{\pi 2} (1 - \phi_i^2) h(\pi_2) \tag{4.10}$$

$$\gamma_{\pi 2} = -m(z - z_0) + \gamma_2 \tag{4.11}$$

After the micropipettes are added to the erythrocytes, the simulation runs, still with $v_{\pi i} = 0$, until the volume of the erythrocyte that is inside the micropipette is constant, which means that the cell stops entering the micropipette. After this volume is stabilized it is possible to add the velocity to the simulation.

Since during the micropipette aspiration assay, there is a feedback mechanism

that ensures that the pressure inside the micropipette remains constant throughout the experiment, it was also necessary to simulate a similar mechanism. This mechanism was simulated by measuring the distance that the erythrocyte traveled inside the micropipette. If this distance is below a certain threshold then a velocity is added to the cell so the erythrocyte moves inside the micropipette (expression 4.12).

$$-\vec{v}_{inside_{\pi 2}} \cdot h(\pi_2) \cdot \nabla\phi \tag{4.12}$$

During the simulation, it is also possible to calculate the force that one erythrocyte applies on the other. This force can be calculated using equation 4.13. The force described in this equation is the force applied on the erythrocyte on the left (that remains static) by the erythrocyte on the right (it is possible to see which erythrocyte is ϕ_1 and ϕ_2 on figure 4.1. To calculate the force applied by the erythrocyte on right by the erythrocyte on the left the variables ϕ_1 and ϕ_2 should be exchanged in equation 4.13.

$$\vec{F} = -\int \frac{3}{4}\phi_1 \nabla(\gamma(1-\phi_1^2)h(\phi_2) - \eta(1-\phi_1^2)\nabla^2 h(\phi_2))d\vec{r} \tag{4.13}$$

4.4 Initial conditions

The initial values for the different variables for the simulation of the micropipette aspiration assay can be found in table 4.2. These values are adapted from [8], with the exception of S_{target} and V_{target} that result from the simulation of erythrocyte shape.

The model created was simulated in a 3D box of size $14.45(x) \times 14.45(y) \times 10.2(z)\mu\text{m}^3$ and the velocity was applied in the z direction.

Table 4.2: Initial model parameters for the simulation of erythrocytes shapes

Variable	Initial value
M	7.4×10^{-1} m^3/Js
k_B	432 J/ m^3
ϵ	0.17 μm
γ	138×10^{-1} J/m^3
η	0 J/m
α_S	1.8×10^{-5} J/mm^4
S_{target}	6775
α_V	5.9×10^{2} J/mm^6
V_{target}	32390
K_B	2×10^{-18} aJ
v	0.57 μm/s
$\gamma_{\pi 1}$	30
$\gamma_{\pi 2}$	given by equation 4.11

The shape of the erythrocytes can be obtained from the integration of the equation 4.14, with η obtained from equation 4.6. This was possible by using a semi-implicit method to integrate the equations throughout the simulation model, where the non-linear terms were initially calculated in real space and then the FFT algorithm was used to obtain the Fourier Transform of these terms. The next iteration values for the order parameters, ϕ_1 and ϕ_2 were calculated in Fourier space and the inverse FFT algorithm was used to calculate the order parameters back on the real space. A similar approach was used to simulate the micropipettes.

$$\frac{\partial \phi_1}{\partial t} = -M\mu \tag{4.14}$$

4.5 Schematic representation of the simulation model

Figure 4.1 represents the simulation model described in this chapter, in 2D (figure 4.1a) and 3D (figure 4.1b). ϕ_i and ϕ_2 represent each erythrocyte. During the simulations, the velocity was applied to ϕ_1. To both erythrocytes, π_1 represents the wall of the micropipette and π_2 the space inside.

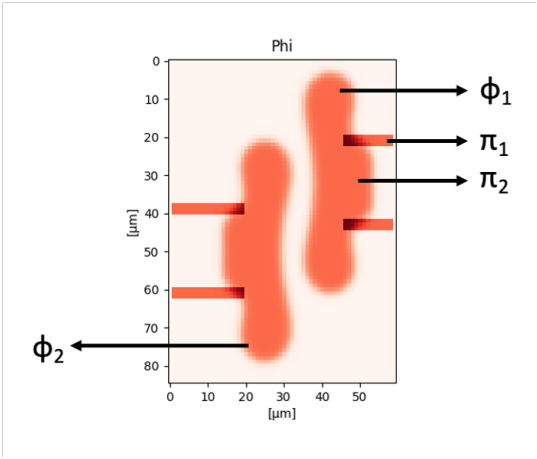

(a)

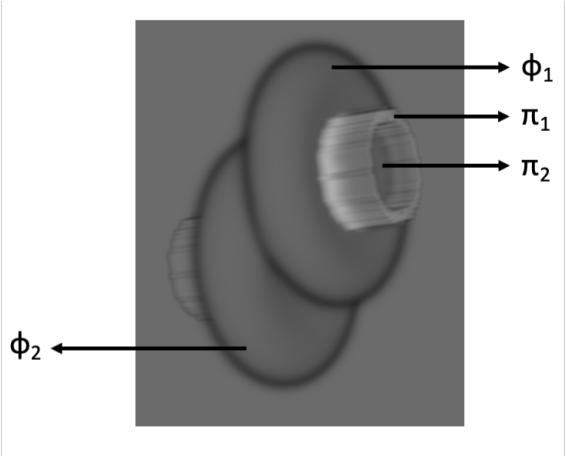

(b)

Figure 4.1: Schematic representation of the model described: (a) 2D model and (b) 3D model

5

Results and Discussion

In this chapter the results obtained from the simulation model described in chapter 4 will be presented.

5.1 Erythrocytes

The biconcave shape of the erythrocyte shape was simulated using equation 4.1. The starting point was an ellipsoid shape. The position of the erythrocytes is given by the center chosen for the ellipsoid. Different simulations were run for erythrocytes aligned along the z axis (figure 5.1) and for erythrocytes not aligned along the z axis (figure 5.2). In both of these cases, they are aligned along the x and y axis. Even though it was not done, it is possible to change these in order to access how the alignment along the order axis can affect the adhesion between the erythrocytes.

As was explained in previous sections, the order parameters ϕ_1 and ϕ_2 have a value of $+1$ inside the erythrocyte and -1 outside the erythrocyte, while it varies near the membrane. This variation can seen more easily in figures 5.1a, 5.1b, 5.2a and 5.2b, due to the differences in shades of red represented.

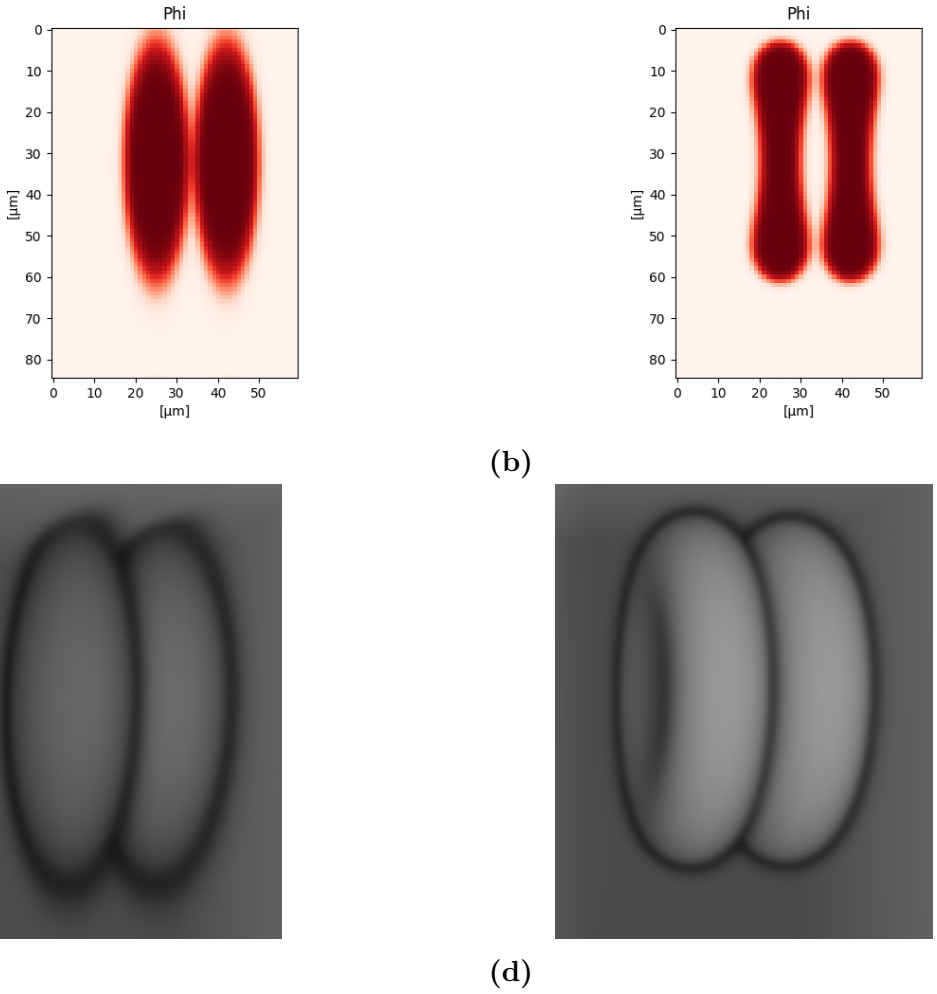

(a) **(b)**

(c) **(d)**

Figure 5.1: 2D and 3D images of the simulation of the initial conditions (a, c) and final shape of the erythrocytes (b, d) when they are aligned along the z axis

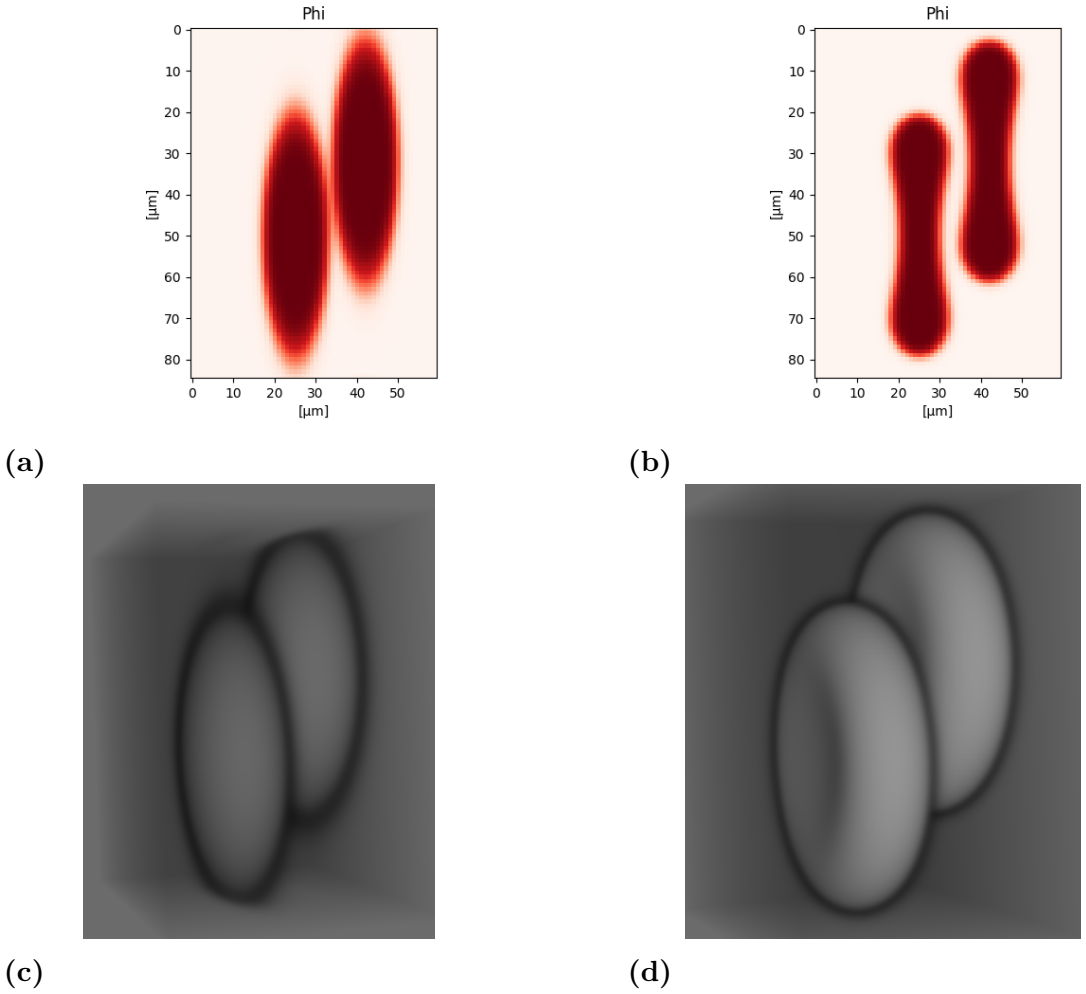

(a) (b)

(c) (d)

Figure 5.2: 2D and 3D images of the simulations of the initial conditions (a,c) and final shape of the erythrocytes (b, d) when they are not aligned along the z axis

5.2 Navier-Stokes velocity equation

After the erythrocytes were simulated, the contribution of the velocity calculated through the Navier-Stokes equations was evaluated. This was achieved by running the simulation model, with the Navier-Stokes velocity, for different values for the fluid viscosity.

(a)

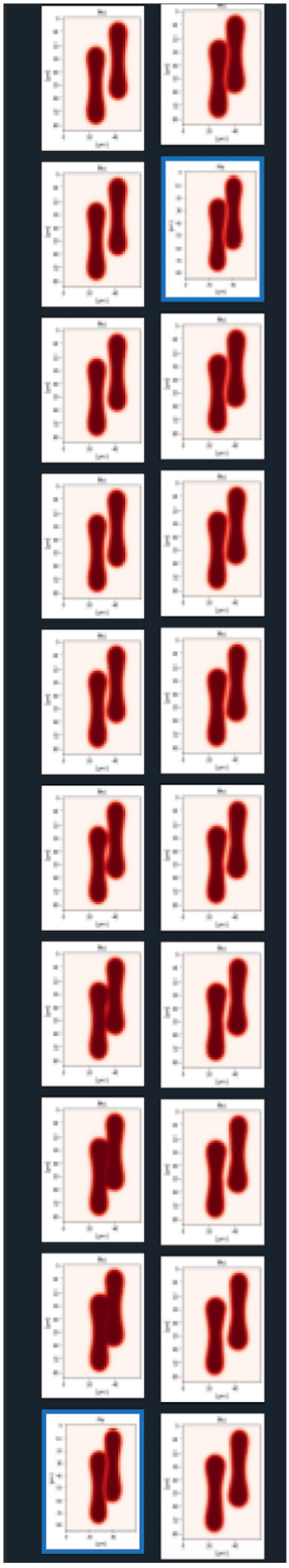

(b)

(c) **(d)**

Figure 5.3: Sequence of images (top to bottom, left to right) of the simulation for different values of fluid viscosity: a)10; b)10^{-2}; c)10^{-7}; d)10^{-20}

Figure 5.3 shows a sequence of images of the simualtion for different values of fluid viscosity with the Navier-Stokes velocity. These values are increasingly smaller, and it is possible to observe that only when the viscosity is smaller than 10^{-20}, does the Navier-Stokes velocity influence the overall result of the simulation. Since it is such a small value it is possible to conclude that the viscosity contribution to the advection velocity is very small and can be neglectable (like it was explained in section 4.2).

5.3 Micropipettes

After the simulation of the erythrocytes' shape, it was necessary to simulate the micropipettes. Figure 5.4 represents the wall of a micropipette.

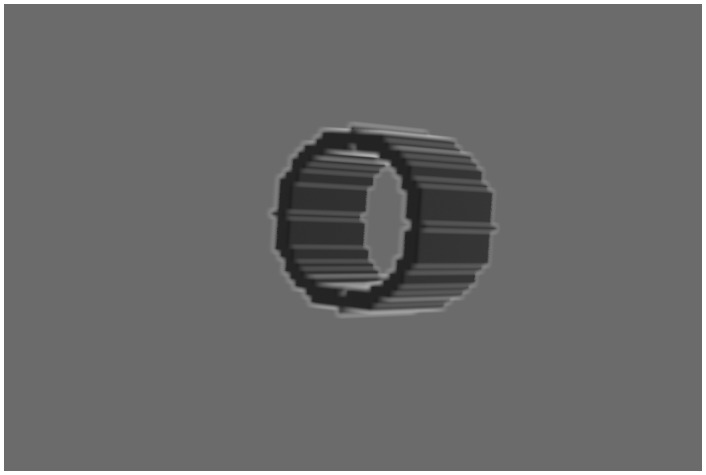

Figure 5.4: Wall of a micropipette for one of the erythrocytes (in 3D image)

Figure 5.5 shows the linear variation of $\gamma_{\pi 2}$, represented for the erythrocyte on the left. The higher value in the middle ensures that the erythrocyte enters the micropipette. In contrast, the lower values ensure that the volume of the erythrocyte inside the micropipette remains constant after a certain amount of time has passed and the erythrocyte is not sucked into the micropipette.

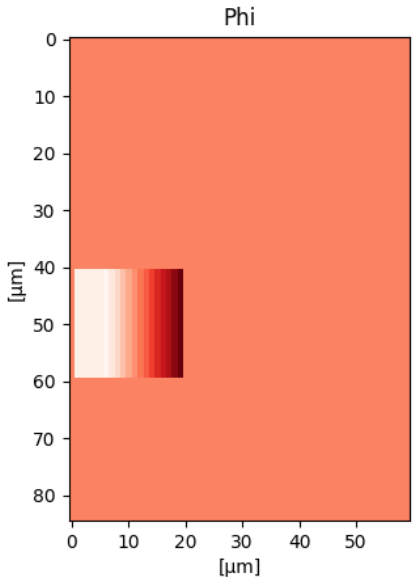

Figure 5.5: Values of $\gamma_{\pi 2}$ in 2D for the erythrocyte on the left. The darkest shade of red shows the place where the micropipette is in contact with the erythrocyte and the value of $\gamma_{\pi 2}$ is higher, ensuring that the erythrocyte enters the micropipette while the lightest shades (white and near white) show that this value decrease with distance, ensuring that the erythrocyte is not sucked into the micropipette.

5.4 Erythrocytes with the micropipettes

As mentioned before, the first step after adding the erythrocytes to the micropipettes was to stabilize the volume of the cell inside the micropipette. This volume depends on the maximum value of $\gamma_{\pi 2}$, when this value is higher, a bigger fraction of the erythrocyte volume stays inside the micropipette. Several values for $\gamma_{\pi 2}$ were tested on several simulations. Some of the results are shown in figure 5.6. Figures 5.6a and 5.6c show the erythrocyte on the left entering the micropipette for different maximum values of $\gamma_{\pi 2}$, while figures 5.6b and 5.6d show the respective graphics of the volume inside of the micropipette as a function of time.

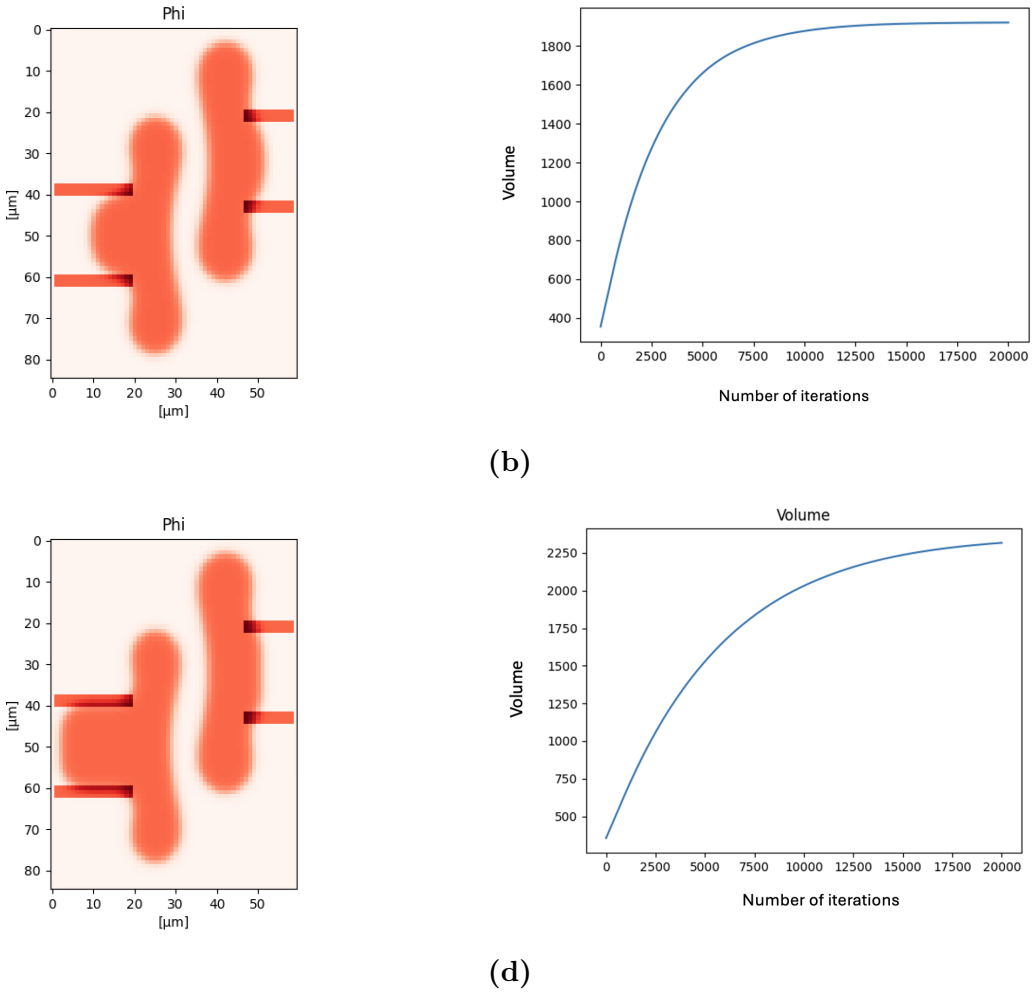

Figure 5.6: Mid-slice profile (a and c) and graphic (b and d) of the stabilization of the volume of the erythrocyte on the left inside of the micropipette for different maximum values of $\gamma_{\pi 2}$. Maximum values of $\gamma_{\pi 2}$: a) 35; b)35; c)45; d) 45

The maximum value used in the next steps of the simulations was 30, since it was the value that allowed to achieve the results closest to the micropipette aspiration assay. The results shown in figure 5.7 correspond to this value of $\gamma_{\pi 2}$. Figure 5.7a and figure 5.7b represent the shape of the erythrocyte after being pushed inside the micropipette as a mide-slice profile and in 3 dimensions, respectively. Even though in figure 5.7a the erythrocytes are not aligned and in figure 5.7b they are, the volume of the cell inside the micropipette is the same. The graphic in figure 5.7c shows the volume of the erythrocyte inside of the micropipette as a function of the time of the simulation and it permits to observe the stabilization of this volume after a certain time has passed.

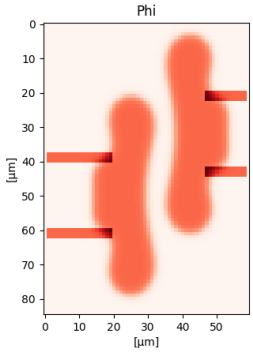

(a)

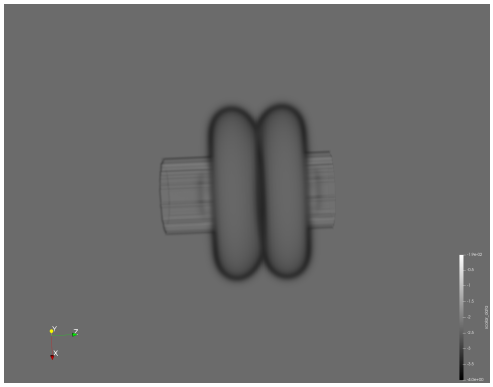

(b)

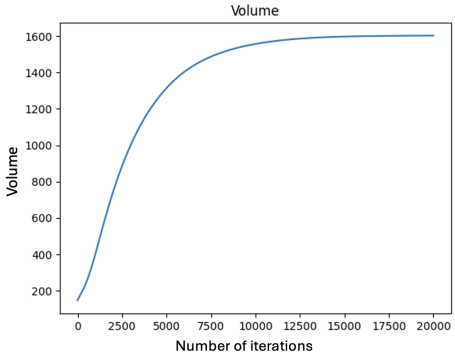

(c)

Figure 5.7: Stabilization of the volume of the erythrocytes inside of the micropipette ($\gamma_{\pi 2} = 30$). a) Erythrocytes inside the micropipettes (2D view); b) Erythrocytes inside the micropipettes (3D view); c) Graphic of the volume of the erythrocyte inside the micropipette as a function of time

After the volume of the erythrocyte inside the micropipette remains constant it is possible to add the velocity to one of the micropipettes (represented on the right). Figure 5.8 shows a sequence of images of the simulation of the micropipette aspiration assay when the erythrocytes are aligned. The figures on the left side

show a mid-slice profile while the figures on the right side show the corresponding 3D representation.

Figures 5.8a and 5.8b show the initial moment, before any velocity is applied. In figures 5.8c and 5.8d, the velocity was already applied to the erythrocyte on the right and it is possible to observe that the erythrocytes are brought together against each other. Figures 5.8e and 5.8f shows the moment where the erythrocytes are rapidly pulled back after of the velocity is changed to start separating the erythrocytes. Figures 5.8g and 5.8h show the beginning of the separation of the erythrocytes, while figures 5.8i and 5.8j show the erythrocytes separate.

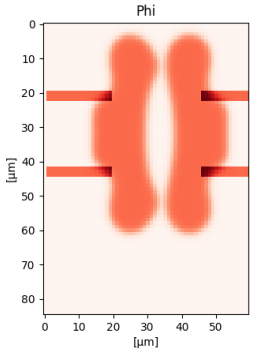

(a)

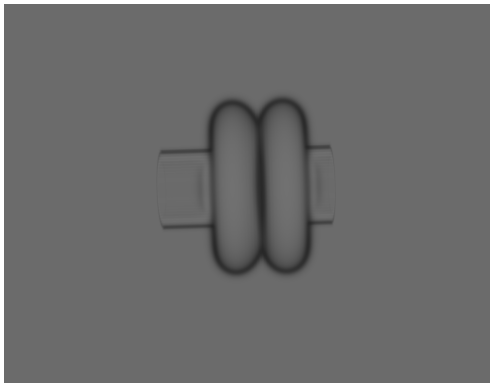

(b)

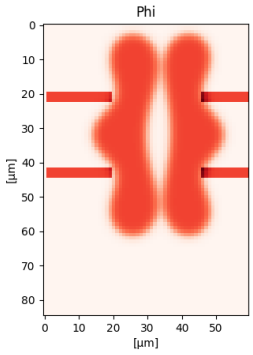

(c)

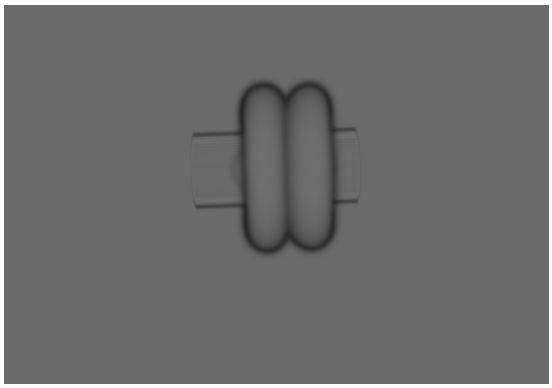

(d)

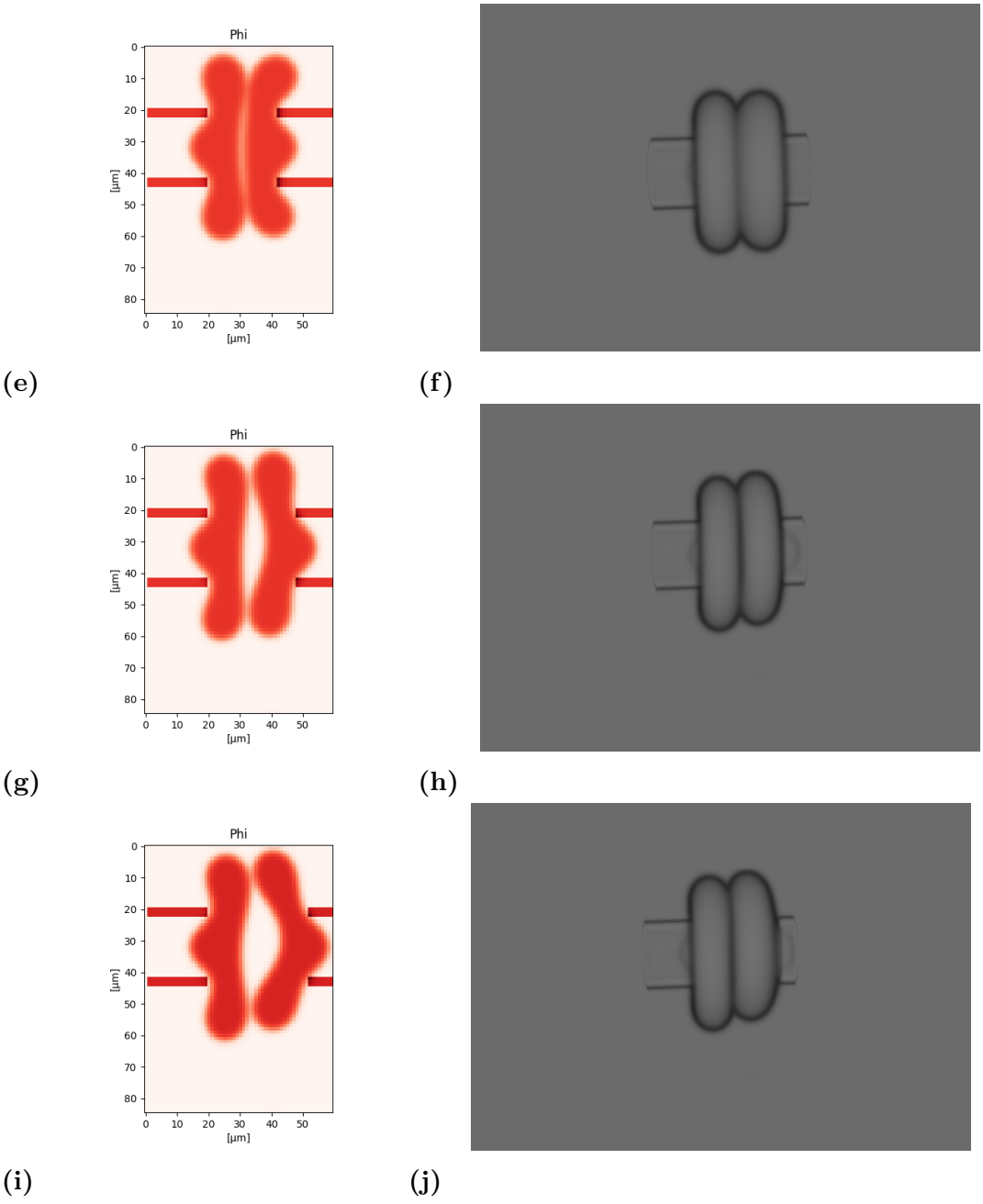

Figure 5.8: Simplified sequence of images of the simulation of the micropipette aspiration assay when the erythrocytes are aligned. The figures on the left side show a mid-slice profile while the right side shows the corresponding 3D representation

During the simulation, it is possible to calculate the force that one erythrocyte applies on the other (equation 4.13). Figure 5.9 is a graphic representation of the force that the erythrocyte on the right applies on the erythrocyte on the left.

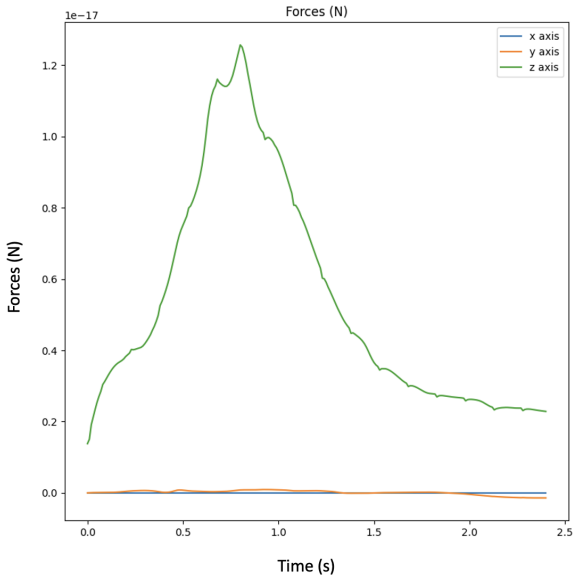

Figure 5.9: Graphic representation of the force that the erythrocyte on the right applies on the erythrocyte on the left as a function of time

Since the erythrocytes are aligned along the x and y axis, the forces along these axes are near constant zero throughout the whole simulation. However, along the z axis the erythrocytes feel a strong repulsive force as they approach each other, which can be seen by the peak in figure 5.9. This force (regulated by the hard-core repulsion coefficient, γ, in equation 4.14), peaks when the erythrocytes are pushed against each other. When the erythrocytes start to separate each from each other the value from the repulsive force decreases. In this simulation, the value of the mobility, M, is relatively small and the erythrocyte relaxes slowly. For that reason, when the cell is pushed backward by the micropipette the regions of the cell further from the micropipette move slowly. In the future, to add adhesion to the simulation, we need to increase the mobility of the system.

6

Conclusion and Future Work

The main goal of this thesis was to develop a mathematical model to simulate the erythrocyte shape as a function of the force applied, the adhesion between the two erythrocytes, and the mechanical characteristics of the cell membrane in the context of a micropipette aspiration assay. Considering this objective and the results presented in chapter 5, it is possible to conclude that the simulation model developed is on track to the proposed goal.

This model was able to simulate the different components necessary to conduct a micropipette aspiration assay, such as the simulation of the erythrocytes, of the micropipettes, and of the feedback mechanism that allows the erythrocytes to remain inside the micropipette. Also it simulates the different steps of the micropipette aspiration assay: the erythrocytes were pushed inside the micropipette, the velocity was added to one of the micropipette until the erythrocytes adhere to each other and, finally its direction of movement was changed to separate the erythrocytes. In addition to this, the model also permits the calculation of the force applied by one of the erythrocytes on the other. In the future we will increase the mobility so the cells respond faster when pulled backwards.

The simulation described in chapter 4 is also simple enough to allow changes in the initial conditions such as the relative positions of the erythrocytes or of the micropipettes. It is also possible to easily change the value of the cell-cell adhesion coefficient (in equation 4.14) in order to simulate different conditions, such as different concentrations of fibrinogen, which could allow the study of new diagnostic methods for vascular diseases.

Some possible future work would be to make an extensive comparison between the results obtained by the simulation model described and the images obtained during the micropipette aspiration assay. In addition, it would also be possible to run more simulations with different initial conditions, such as, the erythrocytes being off-center along the x and y axis, or along more than one axis, as well as simulate different parameters and concentrations of fibrinogen in order to further

analyze how these affect the adhesion force between two erythrocytes.

Bibliography

[1] C. Swenty and M. Hall, "Peripheral vascular disease," *Home Healthc Now*, 2020 Nov/Dec;38(6):294-301.

[2] A. R. Naylor, "Why is the management of asymptomatic carotid disease so controversial?," *The Surgeon*, vol. 13, no. 1, pp. 34–43, 2015.

[3] J. L. Halperin, "Evaluation of patients with peripheral vascular disease," *Thrombosis Research*, vol. 106, no. 6, pp. V303–V311, 2002.

[4] M. Zabczyk, J. Natorska, and A. Undas, "Fibrin clot properties in atherosclerotic vascular disease: From pathophysiology to clinical outcomes," *Journal of Clinical Medicine*, vol. 10, no. 13, 2021.

[5] https://theinternationalmedicine.com/wp-content/uploads/2023/02/Atherosclerosis.jpg. Accessed: 30-07-2023.

[6] M. M. Aleman, B. L. Walton, J. R. Byrnes, and A. S. Wolberg, "Fibrinogen and red blood cells in venous thrombosis," *Thrombosis Research*, vol. 133, pp. S38–S40, 2014. Proceedings of the 7th Symposium on Hemostasis: Old System, New Players, New Directions, May 15-17, 2014, Chapel Hill, North Carolina, USA.

[7] E. Pretorius, O. ofe O. Olumuyiwa-Akeredolu, S. Mbotwe, and J. Bester, "Erythrocytes and their role as health indicator: Using structure in a patient-orientated precision medicine approach," *Blood Reviews*, vol. 30, no. 4, pp. 263–274, 2016.

[8] C. Lopes, J. Curty, F. Carvalho, A. Hernández-Machado, K. Kinoshita, N. Santos, and R. Travasso, "A mathematical model of fibrinogen-mediated erythrocyte–erythrocyte adhesion," *Communications Biology 6*, 192 (2023).

[9] A. F. Guedes, C. Moreira, J. B. Nogueira, N. C. Santos, and F. A. Carvalho, "Fibrinogen–erythrocyte binding and hemorheology measurements in

the assessment of essential arterial hypertension patients," *Nanoscale*, vol. 11, pp. 2757–2766, 2019.

[10] D. H. Farrell, " fibrinogen as a novel marker of thrombotic disease," *Clinical Chemistry and Laboratory Medicine (CCLM)*, vol. 50, no. 11, pp. 1903–1909, 2012.

[11] F. A. Carvalho, S. Connell, G. Miltenberger-Miltenyi, S. V. Pereira, A. Tavares, R. A. S. Ariëns, and N. C. Santos, "Atomic force microscopy-based molecular recognition of a fibrinogen receptor on human erythrocytes," *ACS Nano*, vol. 4, no. 8, pp. 4609–4620, 2010. PMID: 20731444.

[12] M. Zabczyk, R. A. S. Ariëns, and A. Undas, "Fibrin clot properties in cardiovascular disease: from basic mechanisms to clinical practice," *Cardiovascular Research*, vol. 119, pp. 94–111, 01 2023.

[13] S. Herrick, O. Blanc-Brude, A. Gray, and G. Laurent, "Fibrinogen," *The International Journal of Biochemistry Cell Biology*, vol. 31, no. 7, pp. 741–746, 1999.

[14] "fibrin in blood clotting," *Encyclopædia Britannica*.

[15] K. Bridge, H. Philippou, and R. Ariëns, "Clot properties and cardiovascular disease," *Thromb Haemost. 2014 Nov;112(5):901-8.*

[16] J. Klovaite, B. G. Nordestgaard, A. Tybjærg-Hansen, and M. Benn, "Elevated fibrinogen levels are associated with risk of pulmonary embolism, but not with deep venous thrombosis," *American journal of respiratory and critical care medicine*, vol. 187, p. 286—293, February 2013.

[17] A. Guedes, F. Carvalho, I. Malho, and et al., "Atomic force microscopy as a tool to evaluate the risk of cardiovascular diseases in patients," *Nature Nanotech 11*, 687–692 (2016).

[18] F. Campelo and A. Hernández-Machado, "Dynamic model and stationary shapes of fluid vesicles," *Eur. Phys. J. E 20, 37–45 (2006).*

[19] B. Seguin and E. Fried, "Microphysical derivation of the canham–helfrich free-energy density," *Journal of mathematical biology*, vol. 68, 02 2013.

[20] B. Seguin and E. Fried, "Calculating the bending moduli of the canham–helfrich free-energy density," pp. 345–361, 2015.

[21] W. L. Hosch, "Navier-stokes equation," *Encyclopedia Britannica*, 28 Aug. 2023.

[22] S. R. Jain, B. S. Paradkar, and S. M. Chitre, "Low reynolds number flows," pp. 79–98, 2022.

[23] E. Guyon, J.-P. Hulin, L. Petit, and C. Mitescu, "Flows at Low Reynolds Number," 01 2015.

[24] J. Semmlow, "Chapter 3 - fourier transform: Introduction," pp. 81–129, 2012.

[25] W. van Drongelen, "Chapter 6 - continuous, discrete, and fast fourier transform," pp. 103–118, 2018.

[26] M. Müller, "The fourier transform in a nutshell," pp. 39–57, 08 2015.

[27] W. Cochran, J. Cooley, D. Favin, H. Helms, R. Kaenel, W. Lang, G. Maling, D. Nelson, C. Rader, and P. Welch, "What is the fast fourier transform?," *Proceedings of the IEEE*, vol. 55, no. 10, pp. 1664–1674.

[28] E. O. Brigham and R. E. Morrow, "The fast fourier transform," *IEEE Spectrum*, vol. 4, no. 12, pp. 63–70.